A MOLECULAR DYNAMICS STUDY ON SLOW ION INTERACTIONS WITH THE POLYCYCLIC AROMATIC HYDROCARBON MOLECULE ANTHRACENE

Postma, J.; Hoekstra, Romke; Tielens, A. G. G. M.; Schlathölter, Thomas

Published in:
The Astrophysical Journal

DOI:
10.1088/0004-637X/783/1/61

The Astrophysical Journal, 783:61 (10pp), 2014 March 1 doi:10.1088/0004-637X/783/1/61

A MOLECULAR DYNAMICS STUDY ON SLOW ION INTERACTIONS WITH THE POLYCYCLIC AROMATIC HYDROCARBON MOLECULE ANTHRACENE

J. Postma[1], R. Hoekstra[1], A. G. G. M. Tielens[2], and T. Schlathölter[1]
[1] KVI Atomic and Molecular Physics, University of Groningen, Zernikelaan 25 NL-9747 AA Groningen, The Netherlands; t.a.schlatholter@rug.nl
[2] Leiden Observatory, Niels Bohrweg 2, NL-2333 CA Leiden, The Netherlands
Received 2013 November 6; accepted 2014 January 15; published 2014 February 13

ABSTRACT

Atomic collisions with polycyclic aromatic hydrocarbon (PAH) molecules are astrophysically particularly relevant for collision energies of less than 1 keV. In this regime, the interaction dynamics are dominated by elastic interactions. We have employed a molecular dynamics simulation based on analytical interaction potentials to model the interaction of low energy hydrogen and helium projectiles with isolated anthracene ($C_{14}H_{10}$) molecules. This approach allows for a very detailed investigation of the elastic interaction dynamics on an event by event basis. From the simulation data the threshold projectile kinetic energies above which direct C atom knock out sets in were determined. Anthracene differential energy transfer cross sections and total (dissociation) cross sections were computed for a wide range of projectile kinetic energies. The obtained results are interpreted in the context of PAH destruction in astrophysical environments.

Key words: atomic processes – ISM: molecules – molecular data – molecular processes

Online-only material: color figures

1. INTRODUCTION

Polycyclic aromatic hydrocarbon molecules, or PAHs, are thought to be a common molecular constituent of the interstellar medium. They are found in all directions of observation and seem to be distributed over great distance scales. The interstellar medium affects these PAHs through the interstellar radiation field, through stellar winds, shock waves, and hot ionized gas. Since PAHs are observed over great distances, it is of interest to determine their interaction dynamics in these processing mechanisms. This may shed some light on whether PAHs might survive the harsh environments of interstellar space or if they would have to be protectively incorporated into larger (supramolecular) structures in order to survive.

The origin and further (ion-)chemistry of PAHs is not fully understood. One pathway of formation might be that PAHs are formed in regions of high C content through chemical reaction mechanisms as might occur in cool stellar winds (Frenklach & Feigelson 1989). Another proposed mechanism is the erosion of dust grains in shock waves originating for example from supernova explosions (Tielens et al. 1994). PAHs present in these regions are also processed again by the hot post shock gas (Micelotta et al. 2010b). Shock velocities of this kind are relatively low (50–200 km s^{-1}) and since hydrogen and helium are by far the most abundant particles present in the gaseous state (90.8% and 9.1% by number, respectively; Ferriere 2001) in the interstellar medium this suggests an investigation of interactions of ions and PAH molecules in the range of 10–500 eV projectile ion energies.

Over the last two years a number of research groups have started to experimentally study ion interactions with PAHs and PAH clusters. Impact of keV ions such as He^{2+} on anthracene (Postma et al. 2010), pyrene and coronene (Lawicki et al. 2011) was found to efficiently cause multiple ionization followed by extensive fragmentation. PAH ionization and dissociation energies have been determined comparing fragmentation spectra obtained in keV Xe^{q+} collisions with pyrene and fluoranthene with density functional theory calculations (Seitz et al. 2011). Reitsma et al. have experimentally and theoretically determined activation energies (Reitsma et al. 2012) and kinetic energy releases (Reitsma et al. 2013) of anthracene and naphthalene dications, respectively, after ion collisions.

These pioneering studies shed light on the fundamental physics of ion–PAH interactions, however the collision energies under investigation were exceeding the most astrophysically relevant range.

In a recent article Micelotta et al. (2010b) have investigated PAH processing in shocks with velocities between 50 and 200 km s^{-1} using a framework of binary collision approximations (BCA) for the interactions of atomic projectiles and the PAH constituent carbon atoms. It was found that the molecular structure of PAHs is strongly affected by shock processing in the interstellar medium. It is suggested that nuclear interaction could be a pathway to formation of N-containing PAHs. The appeal of the BCA approximation is its straightforward analytical nature. The molecular properties of the target, however, are entirely neglected. A fully realistic description of ion–PAH interactions that includes all molecular properties would require to solve the time-dependent Schrödinger equation for the entire system. Computationally this approach is far too demanding for molecular systems that are more complex than, e.g., H_2. As a feasible alternative, Kunert & Schmidt (2001) have modeled ion collisions with C_{60} molecules using non-adiabatic quantum molecular dynamics (MD) which combines time-dependent density functional theory (TD-DFT) with a classical MD description of the nuclear motion. A similar approach was recently employed by Wang et al. (2011) to study the dynamics of ethylene molecules in intense laser fields. At present the combination of TD-DFT with classical MD is still computationally challenging and very time consuming and thus not an ideal choice for systematic studies of ion–PAH collisions.

We have thus opted for an entirely classical MD approach to study the interactions of hyperthermal to sub-keV H and He atoms with PAHs. As with many other hydrocarbon molecules, the intramolecular forces in PAHs can be modeled realistically using Brenner's analytical bond-order potential (Brenner 1990).

In an early study we have shown that this potential is suitable for studies on ion collisions with free C_{60} molecules (Schlathölter et al. 1999). Note that charge exchange processes are neglected in this study because neutral instead of ionic projectiles are treated.

In this article we present an MD case study on H and He collisions with the PAH anthracene ($C_{14}H_{10}$). After a brief introduction of the interatomic potentials and numerical techniques used, the MD code is validated. In the following, ion induced direct fragmentation and heating of anthracene are investigated and the respective absolute cross sections are derived. The findings are discussed within an astrophysical perspective.

2. SIMULATION

To track the molecular dynamics of the ion–PAH system in time, the classical equations of motion need to be solved numerically for all constituents of the entire collision system. The forces acting on the atomic particles need to be derived from the respective interaction potentials. To obtain optimal results it is crucial to choose a realistic analytical potential, capable of reproducing PAH properties as well as properties of the various possible fragments.

2.1. Intra-molecular Potential

For the intra-molecular potential we use the Brenner reactive bond-order potential, which is based on the pioneering work on (reactive) bond-order potentials by Abell (1985) and Tersoff (1986). Brenner (1990) devised a functional form for the potential, which properly describes radical structures and conjugation and which gives excellent results for a great number of hydrocarbon structures. The potential energy is defined as the sum of an attractive pair potential $V_A(r_{ij})$ and a repulsive pair potential $V_R(r_{ij})$ between the atoms i and j, where r_{ij} is the internuclear distance:

$$E_b = \sum_i \sum_{j>i} V_R(r_{ij}) - \overline{B}_{ij} V_A(r_{ij}). \quad (1)$$

The many-body coupling between the atoms i and j, depending on the local environment of the bond, is included in the bond-order function $\overline{B}_{ij}$. $\overline{B}_{ij}$ explicitly depends on the angles between the ij bond and neighboring bonds ik and jl. Its functional form can be found in Brenner (1990). The pair potentials are defined as

$$V_R(r_{ij}) = f_{ij} \frac{D^e_{ij}}{S_{ij} - 1} e^{-\sqrt{2S_{ij}}\beta_{ij}(r_{ij} - R^e_{ij})}, \quad (2)$$

$$V_A(r_{ij}) = f_{ij} \frac{D^e_{ij} S_{ij}}{S_{ij} - 1} e^{-\sqrt{2/S_{ij}}\beta_{ij}(r_{ij} - R^e_{ij})}. \quad (3)$$

For $S_{ij} = 2$ the sum of these terms equals the Morse-potential (Morse 1929) with a potential well depth D^e_{ij}, an equilibrium internuclear distance R^e_{ij} and a force constant β_{ij}. f_{ij} is a smooth cutoff function to limit the range to nearest neighbors only. The parameters employed here were determined by Brenner (1990) by fitting the free parameters to experimental data.

2.2. Screened Coulomb Interactions

The interaction between fast atomic particles, i.e., between the impinging ion and a PAH constituent atom, can be approximated by a repulsive screened-Coulomb potential:

$$V(r) = \frac{Z_1 Z_2}{r} \Phi(r/a), \quad (4)$$

where Z_1 and Z_2 are the atomic numbers of the collision partners, e is the elemental charge and r the internuclear separation of the particles. The screening function Φ accounts for the action of the electron distributions of the collision partners. The screening length a sets the length scale for this effect. We have chosen the functional form for Φ that was suggested by Ziegler et al. (1985) and that is most widely used for the description of energetic collisions of atomic particles:

$$V(r) = \frac{Z_1 Z_2}{r} \sum_{i=1}^{4} a_i e^{-b_i x}, \quad (5)$$

with

$$x = r/a_U, \quad a_U = \frac{0.8854 a_0}{Z_1^{0.23} + Z_2^{0.23}}. \quad (6)$$

$a_0 = 0.0592$ nm is the Bohr radius. The coefficients in the Ziegler–Biersack–Littmark (ZBL) potential are given in Table 1.

Table 1
ZBL Potential Coefficients a_i and b_i Appearing in the Screening Function

i	a	b
1	0.1818	3.2
2	0.5099	0.9423
3	0.2802	0.4029
4	0.02813	0.2016

2.3. Integration and Validation

To numerically integrate the classical equations of motion, we have employed the particularly accurate Beeman algorithm (Beeman 1976):

$$r(t + \delta t) = r(t) + \delta v(t) + \frac{\delta t^2}{6} [4a(t) - a(t - \delta t)], \quad (7)$$

$$v(t + \delta t) = v(t) + \frac{\delta t}{6} [2a(t + \delta t) + 5a(t) - a(t - \delta t)]. \quad (8)$$

Here v and a are the velocity and acceleration in three dimensions of the particle under study. The algorithm is not self-starting, so to initialize the integration, the velocity-Verlet algorithm (Verlet 1967) was used. The projectile is initialized at a cutoff distance where interaction is negligible and the interaction is tracked until the projectile reaches the cutoff distance again. For perpendicular impact on anthracene, the cutoff distance was chosen to be 35 AU from the molecular plane.

The code was validated by reproduction of the atomization energies calculated by Brenner (1990). The results are shown in Appendix A. A deviation is only found for ethynylbenzene which is probably due to a typo in Brenner's work. Our value of 68.4 eV is in agreement with more recent studies (Che et al. 1999).

The projectile–target interaction was validated by simulating head-on binary collisions for which an analytical solution for the

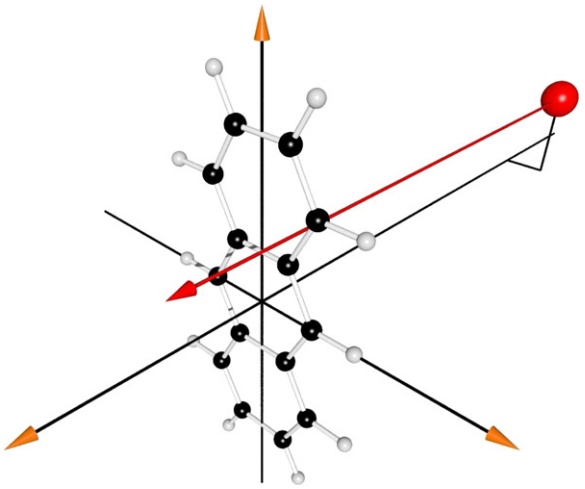

Figure 1. Simulation geometry.
(A color version of this figure is available in the online journal.)

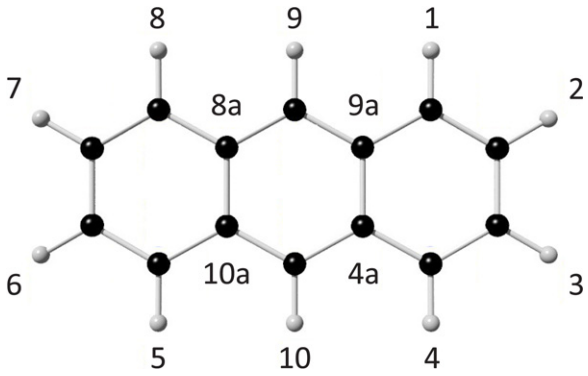

Figure 2. Numbering scheme of atoms in the anthracene molecule.

energy transfer between projectile and target is known (Ziegler et al. 1985):

$$T_m = \frac{4M_pM_t}{(M_p + M_t)^2} E_0 \equiv \gamma E_0, \quad (9)$$

where M_p and M_t are the projectile and target masses respectively, E_0 is the initial projectile kinetic energy and T_m is the maximum transferred energy of the projectile to the target particle. Excellent agreement was found. The simulation geometry used in the following consists of an anthracene molecule and a projectile atomic particle as displayed in Figure 1.

3. RESULTS AND DISCUSSION

3.1. H and He Collisions with Anthracene: Direct Fragmentation

Figures 7 and 8 (Appendix B) show a series of frames of a He projectile colliding head-on with a C atom in the anthracene molecule. The frames are separated in time by 1000 AU = $2.42 \cdot 10^{-14}$ s. The He kinetic energies for these trajectories are $E_{kin} = 40$ eV (Figure 7) and 50 eV (Figure 8), respectively. Clearly at 40 eV, the molecule is left vibrationally excited, but intact whereas at 50 eV the direct hit to a C atom leads to its ejection.

Figure 2 displays the atom numbering scheme for the anthracene molecule used in the following. For a better insight into the interaction process, first a number of characteristic collision geometries are investigated. Table 2 shows results for the

Table 2
100 eV He on Anthracene: Perpendicular Head-on Collisions

Target	Projectile ΔE_{kin} (eV)	Molecule E_{vib} (eV)	E_{frag} (eV)	Effects
		C atoms		
C3	70.60	16.25	54.35	CH loss
C4	70.57	15.90	54.67	CH loss
C4a	69.77	16.85	52.92	C loss
C10	70.52	15.55	54.97	CH loss
		H atoms		
H3	59.48	5.21	54.27	H loss
H4	59.38	5.17	54.21	H loss
H10	59.27	5.15	54.12	H loss
		CC bonds		
C3-C2	12.18	12.18	...	Bond scission
C4-C3	12.15	12.15	...	Bond scission
C4a-C4	11.44	11.44	...	Bond scission
C4a-C9a	10.59	10.59	...	Bond scission
C4a-C10	11.55	11.55	...	Bond scission
		CH bonds		
C3-H3	25.77	12.30	13.47	H loss
C4-H4	25.74	12.28	13.46	H loss
C10-H10	25.71	12.23	13.48	H loss

Note. The first column contains the target, the second column contains projectile kinetic energy losses ΔE_{kin}, and the third and fourth columns contain the molecular vibrational excitation E_{vib} and the kinetic energy of the fragment(s) E_{frag}, respectively.

situation sketched in Figure 1. The molecule is oriented in the yz-plane and a 100 eV He projectile initially moves toward the molecule in x-direction. The time step was 10 AU = 0.24 fs. Relevant quantities are the projectile kinetic energy loss ΔE_{kin}, the kinetic energy of the knocked-out fragment(s) E_{frag} and the vibrational energy of the remaining molecule E_{vib}. The latter is defined as $E_{vib} = \Delta E_{kin} - E_{frag} - E_{trans}$, with E_{trans} being the translational energy of the remaining molecule after the collision (usually on the order of 1–2 eV). For symmetry reasons only results for impact on C3, C4, C4a, C10, H3, H4, and H10 and at the midpoint of the respective bonds are presented. For each impact site, Table 2 lists ΔE_{kin} (Column 2), E_{vib} (Column 3), E_{frag} (Column 4) and the outcome of the collision (Column 5). Clearly, a substantial amount of the projectile energy is carried away by the knocked-out fragment.

The results for 1 keV He projectiles are shown in Table 3 (time step 1 AU = 0.024 fs). In collisions with such energetic projectiles, much less of the projectile kinetic energy is transferred elastically to the remaining molecule. Instead, in head-on collisions an energetic recoil atom is produced. In collisions with a C atom in the molecule, for example, it is obvious that the C atom is knocked out with a substantial amount of energy, while the hydrogen that was attached to it is more or less stationary and stays in the vicinity of the molecule.

Tables 4 and 5 display the results for 100 eV and 1 keV H impact, respectively (time step 1 AU = 0.024 fs). For through-bond trajectories, no bond scission is observed in either case. Head-on collisions always lead to knock out of the respective atom.

In this context it is of interest to investigate the collision dynamics as a function of projectile atom energy, in particular in the energy range where direct atom knock-out sets in. The

Table 3
Same Setup as Table 2, But for 1 keV He on Anthracene: Perpendicular Head-on Collisions

Target	Projectile $\Delta E_{\rm kin}$ (eV)	Molecule $E_{\rm vib}$ (eV)	$E_{\rm frag}$ (eV)	Effects
		C atoms		
C3	744.82	16.64	C:728.00 H:0.18	C,H loss
C4	744.81	15.34	C:729.30 H:0.17	C,H loss
C4a	744.38	16.09	C:728.28	C loss
C10	744.77	15.02	C:729.58 H:0.17	C,H loss
		H atoms		
H3	635.32	4.95	630.37	H loss
H4	635.25	4.92	630.33	H loss
H10	635.13	4.89	630.24	H loss
		CC bonds		
C3-C2	1.05	1.05	...	...
C4-C3	1.05	1.05	...	...
C4a-C4	0.99	0.99	...	...
C4a-C9a	0.92	0.92	...	...
C4a-C10	1.00	1.00	...	...
		CH bonds		
C3-H3	2.78	2.78	...	...
C4-H4	2.78	2.78	...	...
C10-H10	2.77	2.77	...	...

Table 4
100 eV H on Anthracene: Perpendicular Head-on Collisions

Target	Projectile $\Delta E_{\rm kin}$ (eV)	Molecule $E_{\rm vib}$ (eV)	$E_{\rm frag}$ (eV)	Effects
		C atoms		
C3	27.37	18.68	8.69	CH loss
C4	27.36	17.99	9.37	CH loss
C4a	27.24	21.31	5.93	C loss
C10	27.35	17.28	9.97	CH loss
		H atoms		
H3	90.32	4.95	85.37	H loss
H4	90.15	4.92	85.23	H loss
H10	89.96	4.88	85.08	H loss
		CC bonds		
C3-C2	0.95	0.95	...	...
C4-C3	0.95	0.95	...	...
C4a-C4	0.90	0.90	...	...
C4a-C9a	0.83	0.83	...	...
C4a-C10	0.90	0.90	...	...
		CH bonds		
C3-H3	2.48	2.48	...	...
C4-H4	2.48	2.48	...	...
C10-H10	2.47	2.47	...	...

Note. The first column contains the target, the second column contains projectile kinetic energy losses, and the third and fourth columns contain the molecular vibrational excitation and the energies of the fragments, respectively.

threshold kinetic energy transfer $T_0 = \Delta E_{\rm kin}^{\rm threshold}$ is reached when the hitting atom obtains sufficient momentum to get liberated from the anthracene molecule. The quantity T_0 is often referred to as the vacancy formation energy. T_0 can be determined for a given projectile and impact site by simulation of the respective collision as a function of the projectile kinetic energy.

Table 5
Same Setup as Table 4, But for 1 keV H on Anthracene: Perpendicular Head-on Collisions

Target	Projectile $\Delta E_{\rm kin}$ (eV)	Molecule $E_{\rm vib}$ (eV)	$E_{\rm frag}$ (eV)	Effects
		C atoms		
C3	284.27	15.71	C:268.16 H:0.40	C,H loss
C4	284.27	15.39	C:268.48 H:0.40	C,H loss
C4a	284.26	16.17	C:268.09	C loss
C10	284.27	15.07	C:268.80 H:0.40	C,H loss
		H atoms		
H3	969.85	4.90	964.95	H loss
H4	971.63	4.87	966.76	H loss
H10	971.99	4.84	967.15	H loss
		CC bonds		
C3-C2	0.081	0.081	...	...
C4-C3	0.081	0.081	...	...
C4a-C4	0.077	0.077	...	...
C4a-C9a	0.071	0.071	...	...
C4a-C10	0.078	0.078	...	...
		CH bonds		
C3-H3	0.22	0.22	...	...
C4-H4	0.22	0.22	...	...
C10-H10	0.22	0.22	...	...

In Figure 3 the projectile kinetic energy dependence of $\Delta E_{\rm kin}$, $E_{\rm vib}$, $E_{\rm frag}$ and $E_{\rm trans}$ for collisions of H (blue) and He (red) with the anthracene carbon atom number 4a is depicted. The dashed vertical lines indicate the threshold kinetic energy for direct knock-out $E_{\rm kin}^{\rm threshold}$. Note that prompt bond scission already sets in at projectile energies a few eV below $E_{\rm kin}^{\rm threshold}$. $\Delta E_{\rm kin}$ (Figure 3, top) exhibits an almost linear increase with $E_{\rm kin}$ as expected from classical mechanics. For low projectile kinetic energies, $\Delta E_{\rm kin}$ is almost entirely transferred into $E_{\rm vib}$ ($\approx$95% for H, $\approx$90% for He), which accordingly exhibits an almost linear dependence on $E_{\rm kin}$ as well. Because of the much larger mass of the anthracene molecule as compared to the projectile atom, molecular translational energies $E_{\rm trans}$ stay below 2.5 eV and 2 eV for He and H respectively and increase almost linear with $E_{\rm kin}$.

Molecular excitation exhibits a clear peak at $E_{\rm kin} \approx E_{\rm kin}^{\rm threshold}$, the threshold projectile kinetic energy for carbon knock-out. These values (He: 43 eV, H: 99 eV) are strongly dependent on the projectile mass. Independent from the projectile mass is the quantity $\Delta E_{\rm kin}^{\rm threshold} = T_0$ which amounts to approximately 27 eV (see horizontal line in Figure 3, top). For solid targets T_0 is often referred to as "threshold displacement energy"). It depends not only on the site but also on the orientation and therefore is a rather ill-defined quantity, still experimentally undetermined for free PAHs. Experimental and theoretical determinations of T_0 on solid carbon have yielded numbers ranging from 5 eV for amorphous graphite (Cosslett 1978), over 7.6–15.7 eV for carbon nanotubes (Füller & Banhart 1996), to 15–20 eV for graphitic nanostructures (Banhart 1997). In their BCA study, Micelotta et al. chose a conservative value of $T_0 = 7.5$ eV for most of their calculations, which is in line with the nanotube data. Very recently, however, from first principles density functional theory MD calculations on electron collisions with graphene, a displacement energy $T_0 = 22.03$ eV was obtained (Kotakoski et al. 2010). Calculations using the tight binding approximation found $T_0 = 23$ eV (Zobelli et al.

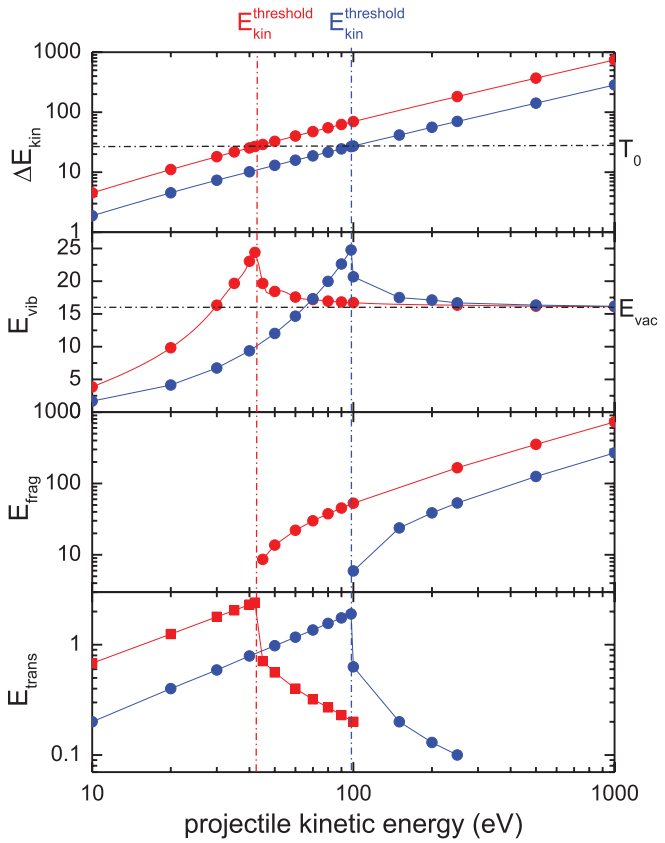

Figure 3. Energetics of H (blue) and He (red) atoms colliding with C4a of anthracene. From top to bottom: total energy loss $\Delta E_{\rm kin}$, anthracene vibrational energy $E_{\rm vib}$, kinetic energy of the knocked out atom(s) $E_{\rm frag}$, and anthracene translational energy $E_{\rm trans}$ (in eV).

(A color version of this figure is available in the online journal.)

2007), whereas classical MD simulations of ion bombardment on graphene with interactions based on the Brenner potential yielded $T_0 = 22.2$ eV (Lehtinen et al. 2010). Using the first principles value $T_0 = 22.03$ eV, experimentally observed cross sections for electron induced knock-out from graphene sheets could be very well reproduced (Meyer et al. 2012).

Tables 6 and 7 display T_0 for perpendicular head-on collisions of H and He projectiles on the different C sites in anthracene obtained from our MD simulation. For comparison, the values for coronene ($C_{24}H_{12}$) and graphene are displayed as well (graphene was simulated as a sheet of 200 C atoms with the impact site in the center). Clearly, very similar values are observed for the two PAHs and for graphene, i.e., the recently obtained threshold displacement energies for graphene can be used as a reference for our data. Our results for graphene are markedly higher than the experimentally determined $T_0 = 22.03$ eV. To some extent, this discrepancy is due to the long range nature of the interaction potentials, which implies an interaction between the incoming ion/atom and typically more than one C atom in the target. Energy is thus also transferred to neighboring C atoms and not only to the knock-out atom. Furthermore, the minimum value for T_0 depends also on the orientation of the system. Direct initialization of the knock out atom with appropriate momentum in the MD code used here gives $T_d \approx 21.3$ eV, which is close to the reference data. It can thus be concluded, that the T_0 values for PAHs displayed in Tables 6 and 7 are realistic.

For projectile kinetic energies exceeding the knock-out threshold the excitation of the molecule decreases asymptotically to the vacancy energy $E_{\rm vac}$. The vacancy energy is a quantity that weakly depends on the C-atom location in the molecule and on the size of the PAH. For C4a in anthracene, $E_{\rm vac} = 16.0$ eV whereas for a coronene inner ring atom, $E_{\rm vac} = 15.3$ eV. In the $E_{\rm vib}$ plot in Figure 3, the vacancy energy ($E_{\rm vac}$) is indicated by a horizontal line.

It is obvious that—particularly close to threshold—the removal of a carbon atom from a PAH molecule implies $E_{\rm vib} > E_{\rm vac}$. The implication of these findings is that the $E_{\rm vib}$ of a PAH after a direct C knock out depends on $E_{\rm kin}$. It starts at the threshold at T_0 and decreases asymptotically with $E_{\rm kin}$ to reach $E_{\rm vac}$.

Table 6
Threshold Kinetic Energies and Kinetic Energy Transfer for Vacancy Formation by H Projectiles in eV

Target	Projectile $E_{\rm kin}$	Projectile $\Delta E_{\rm kin}$ (T_0)	$E_{\rm frag}$	Effect
		Anthracene		
C3	91	−24.8	6.9	CH loss
C4	90	−24.5	5.8	CH loss
C4a	99	−27.0	5.0	C loss
C10	89	−24.2	4.1	CH loss
		Coronene		
C	94	−25.5	4.0	C loss
		Graphene		
C	95	−25.8	4.7	C loss

Note. First column: target site; second column: threshold kinetic energy; third column: threshold kinetic energy transfer to the molecule (T_0); fourth column: fragment kinetic energy; fifth column: effects of the collision. For the graphene calculation, a sheet consisting of 200 C atoms was used.

Table 7
Threshold Kinetic Energies and Kinetic Energy Transfer for Vacancy Formation by He Projectiles in eV (See Table 6 for Details)

Target	Projectile $E_{\rm kin}$	Projectile $\Delta E_{\rm kin}$ (T_0)	$E_{\rm frag}$	Effect
		Anthracene		
C3	42	−27.7	7.1	CH loss
C4	41	−26.9	5.1	CH loss
C4a	43	−27.5	5.4	C loss
C10	41	−26.8	7.8	CH loss
		Coronene		
C	42	−26.7	6.1	C loss
		Graphene		
C	42	−26.7	6.4	C loss

3.2. Monte Carlo Simulations: Cross Sections

Differential cross sections for elastic energy transfer from a projectile atom to an anthracene molecule are obtained by averaging over many collision events where the target molecule is randomly oriented and where the impact parameter is randomly chosen. To this end Monte Carlo simulations of H and He projectiles interacting with the anthracene molecule were performed. These Monte Carlo simulations were performed by implementing a parallelized version of the code on the "Millipede" computer cluster of the Center for High Performance Computing and Visualization of the University of Groningen.

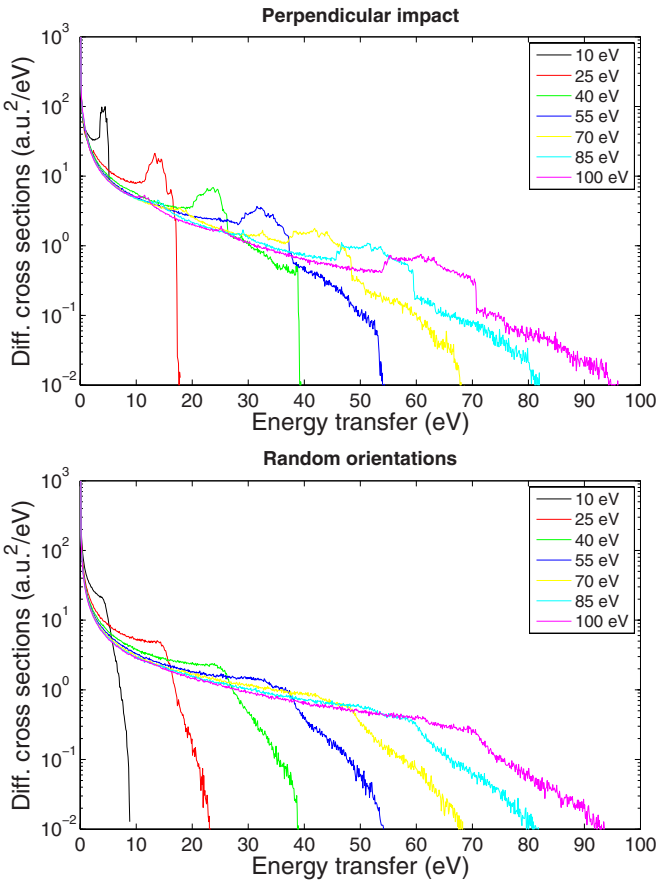

Figure 4. Differential cross sections for energy transfer of He projectiles of various kinetic energies to the anthracene molecule for upright (i.e., projectile trajectories perpendicular to the plane of the molecule) orientation (top panel) and random orientations (bottom panel).

(A color version of this figure is available in the online journal.)

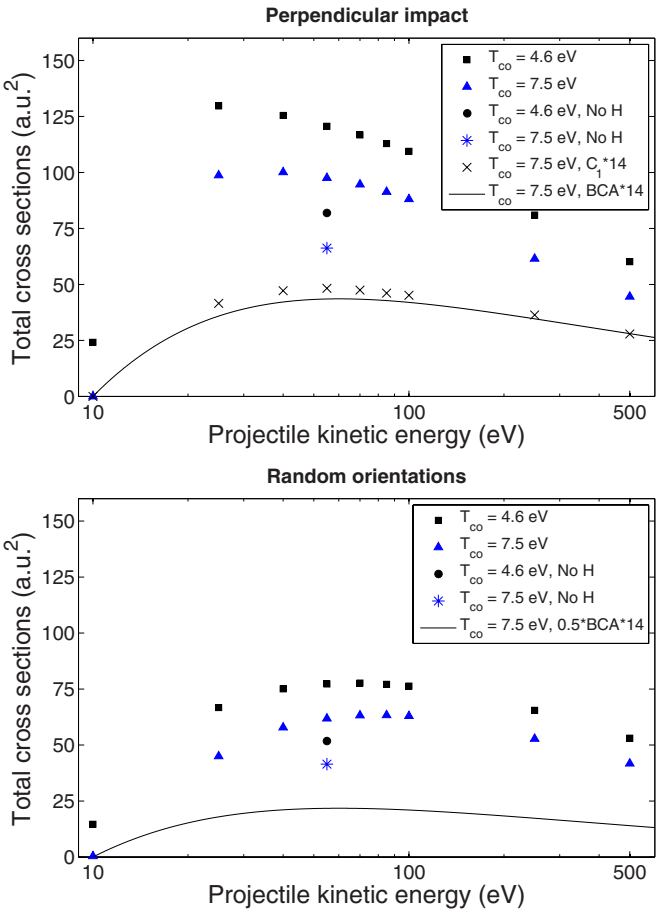

Figure 5. Total cross sections for above threshold energy transfer of He projectiles of various kinetic energies to the anthracene molecule for upright (i.e., projectile trajectories perpendicular to the plane of the molecule) orientation (top panel) and random orientations (bottom panel). The BCA results are added for comparison. For random orientations, the BCA cross section is corrected for orientational averaging to 50% (Micelotta et al. 2010b).

(A color version of this figure is available in the online journal.)

The molecule was positioned at the origin of the simulation geometry with a fixed orientation or with random orientations. The ion started a fixed distance of 35 AU away from the origin to ensure negligible interaction. A great many ion trajectories with random impact parameters were generated in a window of 40 AU by 40 AU. For every ion trajectory the kinetic energy transfer to the molecule was recorded. This allowed for the determination of differential cross sections for energy transfer for a number of projectile kinetic energies of astrophysical interest.

Figure 4 displays differential cross sections for energy transfer (projectile kinetic energy loss) of He atoms of various kinetic energies interacting with anthracene for ion trajectories perpendicular (top panel) to the plane of the molecule and for random orientations (bottom panel), respectively. The differential cross section for energy transfer is defined as

$$\frac{d\sigma}{dE} = \frac{N(E)}{\mathcal{L}\Delta E}, \tag{10}$$

where $N(E)$ is the number of events with energy transfer E, $\mathcal{L}$ is the (time-)integrated luminosity (number of particles per surface area), and ΔE the bin width. The data were binned using bins of 0.1 eV width.

Total cross sections for classes of collisions with energy transfers exceeding a defined threshold can now be computed easily. The values are computed by integrating the differential cross sections using an appropriately chosen lower cut-off value T_{co}. For a better comparison to the BCA results (Micelotta et al. 2010b), it is instructive to choose their knockout energy value of $T_{co} = 7.5$ eV. As already shown, this value falls short of the more realistic knock-out energy, obtained from the MD simulation. However, it is in the range of activation energies for anthracene dissociation. Figure 5 displays absolute cross sections for He impact perpendicular to the PAH plane (top panel) and for random orientations (bottom panel) as a function of projectile energy. In addition, cross sections for $T_{co} = 4.6$ eV are displayed, as this value is the activation energy for the important C_2H_2 loss process. Also shown are the respective data for anthracene targets from which the H atoms were removed, as well as for 14 single non-interacting C atoms, mimicking the anthracene carbon skeleton. The latter data are compared to the BCA results (solid line), representing 14 times the cross section for the above threshold (7.5 eV) energy transfer to an isolated C atom target.

For perpendicular orientation, BCA and MD give almost identical results for the case of 14 C atoms and $T_{co} = 7.5$ eV. When the MD code is run for a target molecule with the H atoms removed, i.e., with a *molecular* carbon skeleton, the total cross sections already exceed the BCA data by about 50% at 55 eV collision energy and $T_{co} = 7.5$ eV. This indicates that the results of the BCA framework cannot immediately and straightforwardly be extrapolated to molecular structures. MD

results for the entire anthracene molecule peak at He collision energies of about 20 eV while the BCA data peaks around 70 eV. At $T_{co} = 7.5$ eV, these MD calculations exceed the BCA data by more than a factor of two. For $T_{co} = 4.6$ eV, the discrepancy amounts to a factor of 3.

Clearly, cross sections drop, when going from a perpendicular collision geometry to random orientations, mainly because of the smaller geometric cross section. In the extreme case of in-plane collisions, projectile interactions only directly affect PAH constituents facing the projectile, while the others are shadowed. This effect is obviously absent in the BCA and MD cases for atomic C. Micelotta et al. therefore corrected BCA cross sections by a factor 0.5 to account for orientational averaging. Including this correction, the discrepancy between MD for the entire molecule and BCA for single atoms would be almost identical in both panels.

In the next section, the cross sections will be used to estimate PAH dissociation cross sections due to excitation by the projectile.

3.3. Dissociation of PAHs

In recent collision studies on anthracene (and other PAH) cations with neutral He at center of mass energies of 110 eV, Stockett et al. observed single C atom loss for all PAHs under study (M. H. Stockett et al. 2014, private communication), which clearly is the experimental signature of the direct knock-out process investigated here. From this experimental study as well as from the MD results presented here, it is however obvious, that direct C knock out is not the main pathway leading to PAH destruction. In photoionization (Jochims et al. 1994), low energy electron impact (Deng et al. 2006), or collision induced dissociation (Arakawa et al. 2000) studies, typically H, H_2, and C_2H_2 loss from singly charged PAH cations are identified as the most important channels and typically no signatures of single C atom loss are observed. These channels and their respective energetics are appropriate for the studies here, as under astrophysically relevant conditions ions rather than neutrals impact on the PAHs, typically leaving the latter positively charged. It is straightforward to assume a statistical process which leads to a scenario in which an excited molecule is subject to competition between two relevant de-excitation mechanisms: infrared (IR) photon emission and dissociation of the molecule.

Once the energy transferred to the molecule (E_{vib}) is known, it is possible to determine a dissociation probability for the molecule if the rates for dissociation and IR-emission are known (Tielens 2005). The dissociation rate can be determined using an Arrhenius relation,

$$k_{diss} = k_0 \exp\left[-\frac{E_0}{k_B T_{eff}}\right], \quad (11)$$

$$T_{eff} \approx 2000 \left(\frac{E_{vib}}{N_C}\right)^{0.4} \left(1 - 0.2\frac{E_0}{E_{vib}}\right),$$

where T_{eff} is the effective temperature of the system, N_C the number of carbon atoms in the molecule, and E_0 the binding energy in eV of the fragment produced in the dissociation process. k_B is Boltzmann's constant. E_{vib} is the excitation energy in eV.

Dissociation competes with successive emission of IR photons of energy ϵ (typically 0.16 eV for a C-C vibrational mode) at a rate k_{IR}, which in turn reduces the molecular excitation energy. This implies that the dissociation probability changes with each IR photon emission. The probability for the excited molecule to dissociate between the nth and $(n + 1)$th IR photon emission equals

$$\phi_n = p_{n+1} \prod_{i=0}^{n} (1 - p_i), \quad (12)$$

where the probability for dissociation at each step is p_i. The unnormalized probability for dissociation at every step p_i equals

$$p_i(E_i) = \frac{k_{diss}(E_i)}{k_{IR}(E_i)}, \quad \text{where} \quad E_i = E_{vib} - i\epsilon, \quad (13)$$

i.e., the ratio of the rate constants for both processes. The total (unnormalized) probability for dissociation of the molecule at the end of the emission chain is the sum of the probabilities for dissociation at each photon emission step. Micelotta et al. assume a constant, average $p_i = p_{av}$ and write the unnormalized total dissociation probability after a maximum of n_{max} photon emissions as (Micelotta et al. 2010a)

$$P(n_{max}) = \sum_{n=0}^{n_{max}} \phi_n \equiv (n_{max} + 1) p_{av} = \frac{k_0 \exp[-E_0/kT_{av}]}{[k_{IR}/(n_{max} + 1)]}. \quad (14)$$

The average temperature T_{av} associated with an average probability p_{av} is taken as the geometric mean $\sqrt{T_{in} \times T_{n_{max}}}$, where T_{in} is the effective temperature immediately after excitation of the molecule by the ion and $T_{n_{max}}$ is the effective temperature after n_{max} IR photon emissions corresponding to an internal energy of $(T_E - n_{max}\epsilon)$. In line with Micelotta et al. (2010a), for anthracene we furthermore assume $n_{max} \approx 3$, $k_{IR} = 100\ s^{-1}$ (Jochims et al. 1994) and $k_0 = 1.4 \times 10^{16}\ s^{-1}$ (Ling & Lifshitz 1998). Of crucial importance is the determination of the Arrhenius energy E_0. By fitting the Arrhenius rate to experimental data from Jochims et al. (1994), Micelotta et al. (2010a) find $E_0 = 3.65$ eV, which is lower than the ≈4.2 eV C_2H_2 binding energy determined for small PAHs (Ling & Lifshitz 1998). For better agreement with astrophysical data, they determine an alternative value of $E_0 = 4.6$ eV (Micelotta et al. 2010a). Note that the determination of E_0 is fundamentally difficult because C_2H_2 loss competes with H and H_2 loss, which have very similar activation energies.

The Monte Carlo calculations yield the distributions of energy E_{vib} transferred to the anthracene molecule, and thus the initial effective temperature T_{in}, for every single collision. Together with $E_0 = 4.6$ eV and setting $n_{max} = 3$ this in turn allows one to determine the anthracene dissociation probability on an event-by-event basis. The dissociation probability is used to calculate total dissociation cross sections by integrating the differential cross sections (for energy transfer of the ion to the molecule) multiplied by the dissociation probability for each energy transfer:

$$P_{diss}(T_E) = \frac{k_0 \exp[-E_0/kT_{av}]}{[k_{IR}/(n_{max} + 1) + k_0 \exp[-E_0/kT_{av}]]}. \quad (15)$$

The dissociation probability is relatively constant over the range of energy transfers at approximately 0.6.

The total dissociation cross section can now be determined for every collision energy. To do so, trajectories leading to direct knock out are not counted separately for two reasons. First of all, direct knock out is only a quantitatively small dissociation channel and second, this channel is associated with relatively

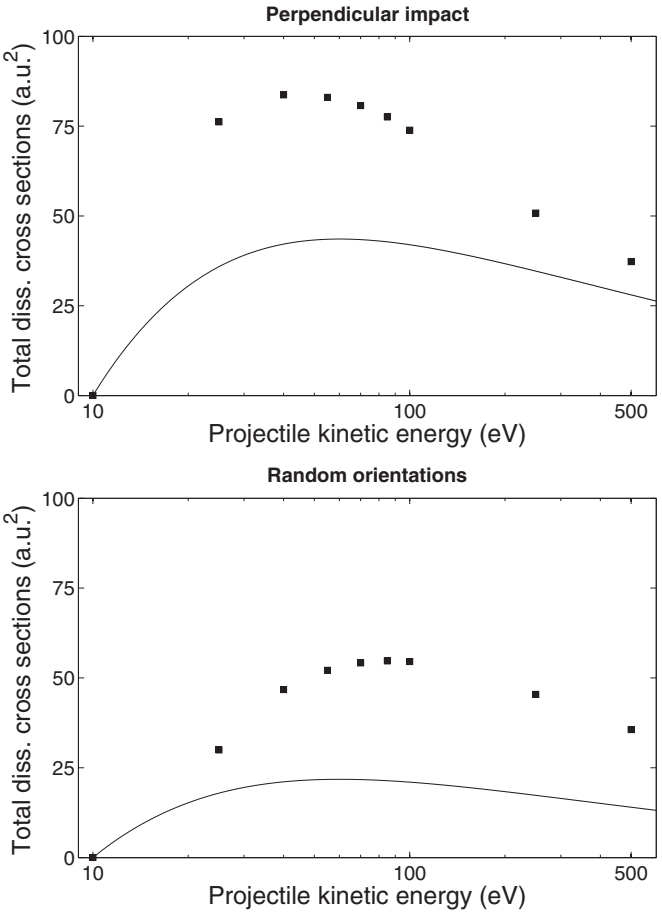

Figure 6. Total anthracene dissociation cross sections after He collisions (squares). The solid line gives the total BCA cross section for collisions leading to excitation energies exceeding $T_{co} = 7.5$ eV. For random orientations, the BCA cross section is corrected for orientational averaging to 50% (Micelotta et al. 2010b).

high excitation energies, leading to subsequent dissociation processes. Figure 6 shows the total dissociation cross sections for perpendicular impact (top panel) and for random molecular orientations (bottom panel). Fortunately, these total dissociation cross sections are not very sensitive to the precise value of the integration lower cut-off of 4.6 eV or 7.5 eV, making the choice of the cut-off value less critical. The reason is the fact that the dissociation probability is close to zero near this threshold.

Micelotta et al. (2010b) have determined PAH dissociation cross sections using the BCA and assuming ion induced C atom knock-out as the underlying mechanism. Knock out was assumed to occur if the transferred energy exceeded a displacement threshold of 7.5 eV. We have already shown that MD calculations reveal a significantly larger displacement energy, but how do the resulting fragmentation cross sections compare?

The knock-out results of BCA calculations for the 7.5 eV threshold from Figure 5 are displayed as a solid line in Figure 6 for comparison. Once again, these values have to be corrected by 0.5 for orientational averaging in the case of randomly oriented targets. It can be seen that for perpendicular impact the MD cross sections exceed the BCA data by almost a factor of 2 for 40 eV projectile energies whereas the curves almost converge at high projectile velocities. For random orientation, cross sections are again markedly lower and the maximum is now observed for

Table 8
Average Energy Transfers for He Projectiles at Various Kinetic Energies Colliding on Anthracene

Projectile E_{kin} (eV)	T_E (eV) This Work ($T_{co} = 4.6$)	T_E (eV) (Micelotta et al. 2010b) $T_{co} = 7.5$
10	5.4	...
25	9.8	12.0
40	14.2	15.2
55	17.6	17.9
70	20.2	20.2
85	22.2	22.3
100	23.9	24.1
250	33.7	36.1
500	42.1	46.1

Note. The second column shows our average energy transfers. The third column gives average energy transfers from the binary collision approximation of Micelotta et al. (2010b).

projectile energies around 100 eV. Here, the dissociation cross section is more than twice as high as the BCA data (corrected for orientational averaging). Differences are smaller for lower and higher projectile energies.

In Table 8 we have made a comparison between the average energy transfer of He projectiles to the anthracene molecule as obtained from our simulations and the BCA of Micelotta et al. (2010b). The average energies obtained in this work are calculated using the lower limit of integration or cut-off of $T_{co} = 4.6$ eV instead of the somewhat artificially chosen lower limit of $T_{co} = 7.5$ eV for direct single carbon knock out, but as the range of energy transfers grows larger this difference is felt less and less. At projectile energies of 55 eV for He the average energy transfers are already very similar.

The astrophysical implications of ion induced PAH destruction in interstellar shocks have been investigated in great detail by Micelotta et al. (2010b). Based on BCA calculations assuming a displacement energy of 7.5 eV, they show that for a PAH containing 50 C atoms, destruction only sets in at shock velocities of about 100 km s^{-1}. For a displacement energy of 15 eV, this value shifts to about 125 km s^{-1}. In the light of the MD calculations, it is clear that the BCA systematically underestimates cross sections for above threshold energy transfer. However, even the displacement energy of 15 eV falls short of the ≈22 eV obtained by MD calculations. We conclude that the results presented here will not significantly change the shock velocity onset for PAH destruction. Electron collisions on the other hand are already very important for shock velocities of 75 km s^{-1} (Micelotta et al. 2010b). The main astrophysical implication of the present study thus is the "outcome" of the collision. Due to the high displacement energies, direct C atom knockout is not a very strong destruction pathway. Destruction proceeds mainly through C_2H_2 loss from the periphery of the PAH. If the PAH is not fully destroyed, C_2H_2 loss can initiate isomerization and cage formation. The small relevance of knock-out collisions on the other hand leaves little room for PAHs with internal vacancies. N atom incorporation at such reaction sites is thus not an obvious pathway toward nitrogenated PAHs.

4. CONCLUSIONS

Using MD simulations, we have studied the interactions of hydrogen and helium atoms with anthracene as prototypical systems for particle collisions with PAH molecules.

Two main conclusions can be drawn from this work.

First, the threshold kinetic energy for a knock-out collision is much larger than estimated previously. With the MD approach, C knock out in a head on collision with the respective C-atom occurs for kinetic energies above 43 eV (He) and 99 eV (H) while BCA calculations find threshold kinetic energies of 10 eV and 26 eV, respectively when assuming a knock-out energy of 7.5 eV (Micelotta et al. 2010b). The reason for the discrepancy is in part due to the fact, that BCA approaches neglect the molecular nature of the PAH. Furthermore, only recently a precise experimental determination of the C threshold displacement energy in graphene bas been obtained (T_0 − 22.03 eV (Meyer et al. 2012)). Our MD approach reproduces this knock out energy. For anthracene, we find appreciable numbers of knock-out events for energy transfer of at least ≈27. Previous studies had to rely on older and much less consistent data, hinting at much lower threshold displacement energies as used in the BCA study. As a consequence, direct C-loss is a weak channel and accordingly this process appears not to provide a route toward incorporation of N atoms into the PAH structure. However, the recent first experimental observation of direct C atom knock out in PAH collisions (M. H. Stockett et al. 2014, private communication) is an important first step toward a detailed understanding of collision induced vacancy production in PAH molecules. Therefore it is now feasible to experimentally test the presented MD results in detail in the region where knock out sets in.

Because direct knock out of C atoms from PAHs did not prove to be an efficient channel toward PAH destruction, we considered the dissociation of PAHs through vibrational excitation, as previously done by Micelotta et al., for electron collisions (Micelotta et al. 2010a). This dissociation channel competes with de-excitation through IR photon emission. The dissociation probability (≈0.6) appears to be quite constant over the range of studied projectile energies. Calculating total dissociation cross sections by weighing the integral over the differential cross section for energy transfer with the dissociation probability for that particular energy transfer gives results that are clearly larger than the results obtained from BCA calculations and a C knock-out model. Total dissociation cross sections do not appear to be very sensitive to the precise lower cut-off value. To summarize, for small PAHs as anthracene, ion processing primarily induces loss of C_2H_2 (or other fragments) rather than C-atom knockout. The corresponding dissociation cross sections exceed those determined from a knock out model and imply a larger role of ionic particles than previously thought. Furthermore, dissociation hints at subsequent isomerization and cage formation, rather than formation of reactive "inner" vacancies, which may act as active sites for PAH nitrogenation.

APPENDIX A

TABLE OF ATOMIZATION ENERGIES

To validate the MD code, atomization energies were computed for all the hydrocarbon compounds that were studied in Brenner's original work (Brenner 1990). Table 9 compares the respective data obtained here with the numbers determined by Brenner and with experimental data. The agreement is excellent with the exception of ethynylbenzene. For this particular compound, Brenner's result is likely to be incorrect, as our value agrees well with more recent studies (Chen et al. 1999).

Table 9
Energies of Atomization (eV) of a Number of Molecular Structures

Structure	This Work	Brenner	Experiment
	Alkanes		
methane	17.57	17.6	17.6
ethane	29.72	29.7	29.7
propane	41.99	42.0	42.0
n-butane	54.26	54.3	54.3
i-butane	54.27	54.3	54.4
n-pentane	66.54	66.5	66.6
isopentane	66.54	66.5	66.6
neopentane	66.79	66.8	66.7
cyclopropane	35.51	35.5	35.8
cyclobutane	48.65	48.7	48.2
cyclopentane	61.35	61.4	61.4
cyclohexane	73.63	73.6	73.6
	Alkenes		
ethylene	23.63	23.6	23.6
propene	36.23	36.2	36.0
1-butene	48.50	48.5	48.5
cis-butene	48.83	48.8	48.6
isobutene	48.39	48.4	48.7
$(CH_3)_2C{=}C(CH_3)_2$	73.15	73.2	73.4
cyclopropene	28.19	28.2	28.8
cyclobutene	42.41	42.4	42.4
cyclopentene	55.75	55.7	55.6
1,4-pentadiene	55.00	55.0	54.8
$CH_2{=}CHCH{=}CH_2$	41.84	41.8	42.6
$CH_3CH{=}C{=}CH_2$	40.42	40.4	42.1
$H_2C{=}C{=}CH_2$	27.82	27.8	29.6
	Alkynes		
acetylene	17.15	17.1	17.1
propyne	29.42	29.4	29.7
1-butyne	41.69	41.7	42.0
2-butyne	41.69	41.7	42.2
	Aromatics		
benzene	57.47	57.5	57.5
toluene	69.63	69.6	70.1
1,4-dimethylbenzene	81.79	81.8	82.6
ethylbenzene	81.90	81.9	82.5
ethenylbenzene	76.19	76.2	76.5
ethynylbenzene	68.39	69.8	69.9
naphthalene	91.39	91.4	91.2
anthracene	125.30	...	...
	Radicals		
CH_2	7.77	7.8	7.8
CH_3	12.71	12.7	12.7
$H_3C_2H_2$	25.67	25.7	25.5
H_2C_2H	18.88	18.9	18.9
C_2H	12.24	12.2	12.2
CH_2CCH	24.45	24.5	25.8
n-C_3H_7	37.94	37.9	37.8
i-C_3H_7	38.25	38.3	38.0
t-C_4H_9	50.47	50.5	50.5
phenyl	72.71	52.7	72.7

Note. The columns "Brenner" and "Experiment" are adopted from Brenner (1990).

APPENDIX B

COLLISION FRAMES

Figures 7 and 8 illustrate the time evolution of a head-on collision process for the example of a He projectile impinging

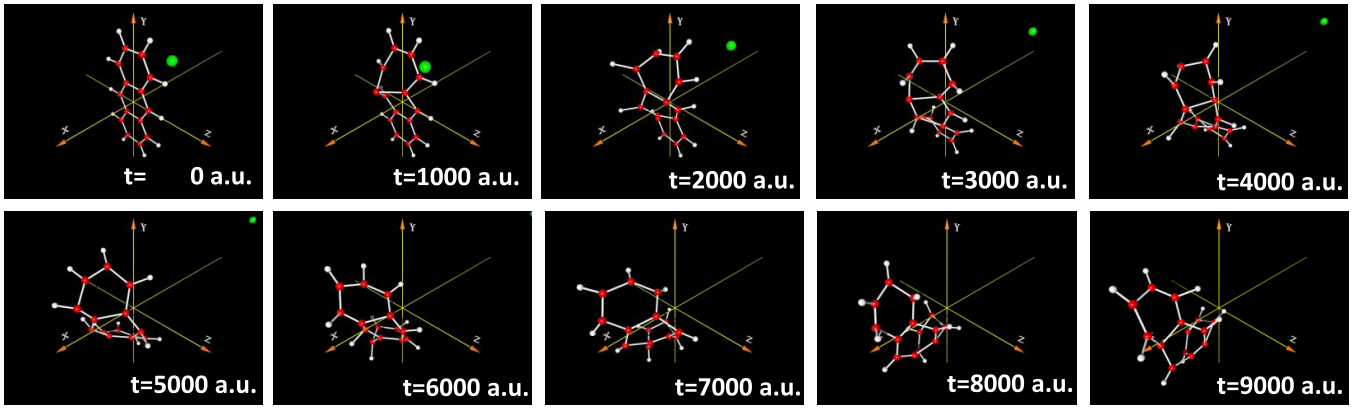

Figure 7. 40 eV He on anthracene: The molecule remains intact.
(A color version of this figure is available in the online journal.)

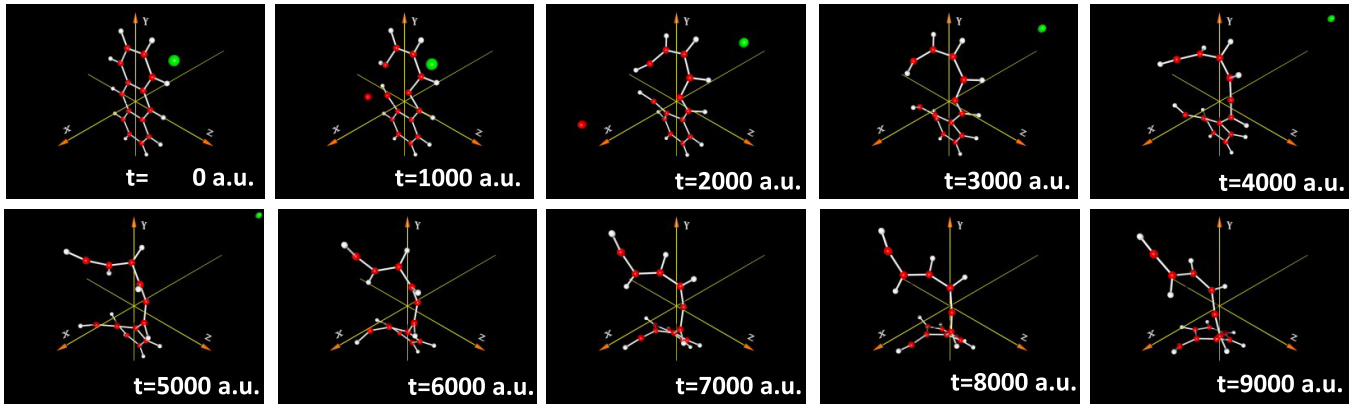

Figure 8. 50 eV He on anthracene. A C atom is knocked out of the molecule. The impact parameter is identical to the one in Figure 7.
(A color version of this figure is available in the online journal.)

onto the anthracene C9a atom with an initial projectile momentum perpendicular to the anthracene plane. The frames are separated in time by 1000 AU $= 2.42 \cdot 10^{-14}$ s. The He kinetic energies for these trajectories are $E_{\rm kin} = 40$ eV (Figure 7) and 50 eV (Figure 8), respectively. Clearly at 40 eV, the molecule is left vibrationally excited but intact, whereas at 50 eV the direct hit to a C atom leads to its ejection.

REFERENCES

Abell, G. C. 1985, PhRvB, 31, 6184
Arakawa, R., Kobayashi, M., & Nishimura, T. 2000, J. Mass Spectrom., 35, 178
Banhart, F. 1997, JAPh, 81, 3440
Beeman, D. 1976, JCoPh, 20, 130
Brenner, D. W. 1990, PhRvB, 42, 9458
Che, J., Çağin, T., & Goddard, W. A., III 1999, Theoretical Chemistry Accounts, 102, 346
Chen, L., Bernard, J., Denis, A., Martin, S., & Desesquelles, S. M. J. 1999, PhRvA, 59, 2827
Cosslett, V. E. 1978, JMic, 113, 113
Deng, Z., Bald, I., Illenberger, E., & Huels, M. A. 2006, PhRvL, 96, 243203
Ferriere, K. M. 2001, RvMP, 73, 1031
Frenklach, M., & Feigelson, E. D. 1989, ApJ, 341, 372
Füller, T., & Banhart, F. 1996, CPL, 254, 372
Jochims, H. H., Rühl, E., Baumgärtel, H., Tobita, S., & Leach, S. 1994, ApJ, 420, 307
Kotakoski, J., Jin, C. H., Lehtinen, O., et al. 2010, PhRvB, 82, 113404
Kunert, T., & Schmidt, R. 2001, PhRvL, 86, 5258
Lawicki, A., Holm, A. I. S., Rousseau, P., et al. 2011, PhRvA, 83, 022704
Lehtinen, O., Kotakoski, J., Krasheninnikov, A. V., et al. 2010, PhRvB, 81, 153401
Ling, Y., & Lifshitz, C. 1998, JPCA, 102, 708
Meyer, J. C., Eder, F., Kurasch, S., et al. 2012, PhRvL, 108, 196102
Micelotta, E. R., Jones, A. P., & Tielens, A. G. G. M. 2010a, A&A, 510, 37
Micelotta, E. R., Jones, A. P., & Tielens, A. G. G. M. 2010b, A&A, 510, 36
Morse, P. M. 1929, PhRv, 34, 57
Postma, J., Bari, S., Hoekstra, R., Tielens, A., & Schlathölter, T. 2010, ApJ, 708, 435
Reitsma, G., Zettergren, H., Boschman, L., et al. 2013, JPhB, 46, 245201
Reitsma, G., Zettergren, H., Martin, S., et al. 2012, JPhB, 45, 215201
Schlathölter, T., Hadjar, O., Hoekstra, R., & Morgenstern, R. 1999, PhRvL, 82, 73
Seitz, F., Holm, A. I. S., Zettergren, H., et al. 2011, JChPh, 135, 064302
Tersoff, J. 1986, PhRvL, 56, 632
Tielens, A. G. G. M. 2005, The Physics and Chemistry of the Interstellar Medium (Cambridge: Cambridge Univ. Press)
Tielens, A. G. G. M., Mckee, C. F., Seab, C. G., & Hollenbach, D. J. 1994, ApJ, 431, 321
Verlet, L. 1967, PhRv, 159, 98
Wang, Z.-P., Dingh, P. M., Reinhard, P. G., Suraud, E., & Zhang, F. S. 2011, IJQC, 111, 480
Ziegler, J. F., Biersack, J. P., & Littmark, U. 1985, in Stopping Powers and Ranges of Ions in Matter, ed. J. F. Ziegler (New York: Pergamon Press), 1
Zobelli, A., Gloter, A., Ewels, C. P., Seifert, G., & Colliex, C. 2007, PhRvB, 75, 245402